Journal of Nuclear Materials 442 (2013) 208–217

Contents lists available at ScienceDirect

Journal of Nuclear Materials

journal homepage: www.elsevier.com/locate/jnucmat

Interaction of a screw dislocation with Frank loops in Fe–10Ni–20Cr alloy

D. Terentyev [a,*], A. Bakaev [a,b,c]

[a] SCK CEN, Boeretang 200, Mol B2400, Belgium
[b] Center for Molecular Modeling, Department of Physics and Astronomy, Ghent University, Technologiepark 903, 9052 Zwijnaarde, Belgium
[c] Department of Experimental Nuclear Physics K-89, Faculty of Physics and Mechanics, St. Petersburg State Polytechnical University, 29 Polytekhnicheskaya Str., 195251 St. Petersburg, Russia

ARTICLE INFO

Article history:
Received 4 March 2013
Accepted 26 August 2013
Available online 31 August 2013

ABSTRACT

The interaction of 2 and 5 nm Frank loops with a moving screw dislocation is studied in Fe–10Ni–20Cr alloy (a model of austenitic 304 and 316 steels) employing the newly developed Fe–Ni–Cr interatomic potential in molecular dynamics simulations. The applied potential ensures full stability of FCC phase and smooth evolution of stacking fault energy (SFE) as a function of chemical composition, fitted to be in a close agreement with the CALPHAD database. A model of Fe–10Ni–20Cr random alloy closely reproduces elastic properties and SFE of 316-type austenitic steels. The results reveal a number of interaction mechanisms depending on loop orientation and ambient temperature. Half of the observed reactions lead to loop unfaulting despite a low SFE of the alloy. The unfaulting reactions are enhanced with temperature and the critical stress for the unfaulting is regularly higher in comparison with the loop shear interaction. By comparing present results with a recent study done in a low SFE Fe–50Ni alloy, we reveal that a magnitude of local variation of SFE is an important factor controlling the formation of dislocation constrictions. In the Fe–50Ni alloy, characterized by strong variations of local SFE, the constrictions are almost never observed so that the loop shear interaction prevails, while absorption is rare. In the Fe–10Ni–20Cr alloy, characterized by small variations of local SFE, the constrictions are regularly formed resulting in frequent loop unfaulting.

1. Introduction

Irradiation of structural steels for nuclear applications by neutrons throughout the lifecycle causes modification of the crystal microstructure resulting in the formation of black dots, dislocation loops and voids [1,2]. These defects act as obstacles to dislocation glide, thereby causing hardening and consequently embrittlement [3], thus limiting the functional lifespan of a setup. In the case of neutron irradiation at temperature below $0.3T_M$ (T_M is the melting point) at a dose up to few (~5), DPAs (displacement per atom), the matrix damage created is composed mainly of dislocation loops with Burgers vector (BV) equal to 1/3<111> (i.e. so called Frank loops) with mean size of a few nm [2,4–6]. Upon plastic deformation, the formation of so called 'free channels' has been observed in austenitic steels with different stacking fault energy (SFE) in [5]. Width, spacing, height and density of channels were found to depend on SFE. The effect of SFE on the interaction of moving dislocations with Frank loops (FL) and formation of free channels therefore needs to be understood as it brings an important contribution to plastic deformation mechanisms and phenomena of plastic localization in irradiated austenitic steels. Given the complexity of the in situ TEM straining experiments (see e.g. [7,8]), molecular dynamics (MD) atomistic simulations offer an efficient complementary tool to investigate the details of dislocation-loop interaction.

FL-dislocation interaction in pure FCC metals (in Cu and Ni) has been studied by MD simulations already [9–11]. A systematic study performed by Nogaret et al. [9] has revealed several mechanisms depending on the interaction geometry and an impinging dislocation character, namely: (i) loop shear; (ii) unfault into glissile configuration; (iii) absorption into a glissile superjog (on edge dislocation) or into a sessile helical turn (on a screw dislocation). Absorption into a helical turn results in especially high unpinning stress and thus is expected to be the main source of hardening. For both screw and edge dislocations the unfaulting mechanism is controlled by the cross-slip process [9,12]. In general, the number of geometrical configurations leading to loop unfaulting is higher for a screw dislocation [9]. Hence, the interaction with screw dislocations most likely determines both the hardening and the formation of free channels.

* Corresponding author.
E-mail address: dterenty@sckcen.be (D. Terentyev).

0022-3115/$ - see front matter © 2013 Elsevier B.V. All rights reserved.
http://dx.doi.org/10.1016/j.jnucmat.2013.08.044

In the case of a screw dislocation, two distinct unfaulting mechanisms have been revealed [10,12]: (i) the formation of a D-Shockley partial dislocation segment, which sweeps the fault. The sweeping is accommodated by cross-slip of the dislocation around the loop. (ii) Cross-slip of the dislocation, formation of a constriction and its re-dissociation in the loop habit plane. Then, two partials remove the fault. Both of these mechanisms require the formation of constrictions and propagation of dislocations in the secondary glide planes. The formation of a constriction on the other hand is determined by the value of SFE and elastic constants of material. Importantly to point that the interatomic models of Ni and Cu, employed in [10,12], are not suitable to mimic properties of dislocations in austenitic steels due to essential discrepancy of SFE and shear modulus. Hence, there is a need for an atomistic model emulating low SFE austenitic steels.

This was addressed recently, by performing MD simulations in Fe–Ni random alloy [13], for which the potential was developed by using BCC-Fe potential by Ackland [14] and FCC-Ni potential from Mishin [15], allowing for SFE to vary in a wide range depending on the alloy's composition. SFE as a function of Ni concentration for the applied Fe–Ni potential is shown in Fig. 1(a). Above 40 at.%, SFE becomes definitely positive demonstrating that FCC phase becomes more stable than BCC. It has been shown that in Fe–50Ni with SFE comparable to real austenitic steels (i.e. ~20 mJ/m^2) [13], the formation of constrictions is suppressed so that unfaulting becomes a less favorable mechanism in comparison with loop shear. At the same time, the presence of a non-negligible friction stress caused by solutes was seen to impede the propagation of dislocations in the secondary glide planes, which is another essential factor suppressing the unfaulting process [13]. The overall conclusion was that in the Fe–50Ni alloy, characterized by SFE of 20 mJ/m^2, the major interaction mechanism is loop shear. Hence, the explanation for the experimental observation of free channels, so far based on the results obtained in pure Cu and Ni in [12], needs further clarification [13].

An important drawback of the Fe–Ni model applied in [13] was a strong variation of SFE depending on local atomic arrangement. The spread of SFE for three different Fe–Ni alloys is shown in Fig. 1(b), simulation details are described in figure capture. Even though the average SFE value in Fe–50Ni is 19 mJ/m^2 the width of the distribution is about 50 mJ/m^2. It is therefore possible that the strong local variation of SFE does not allow for the formation of extended constrictions even at relatively high level of applied shear stress while the FL is in contact with dislocation during the interaction process. The origin of the strong SFE variation is related to a tiny balance in the stability of FCC relative to BCC phase. To overcome this problem, a new Fe–Ni–Cr potential has been developed by utilizing FCC phase as a ground state for Fe, Ni and Cr. By doing that the full stability of FCC phase and smooth evolution of SFE, in a close agreement with the CALPHAD database, were ensured in the whole composition range [16]. In addition, the potential was specifically developed to mimic elastic properties of 316 austenitic steels for 'target composition' i.e. Fe–10Ni–20Cr and was parameterized using a wide range of data including some obtained by *ab initio* calculations and from experiments. Here, we study the interaction of 2 and 5 nm Frank loops with a screw dislocation in Fe–10Ni–20Cr alloy (a model of austenitic 316 steel) employing the newly developed Fe–Ni–Cr interatomic potential whose details are described in [16].

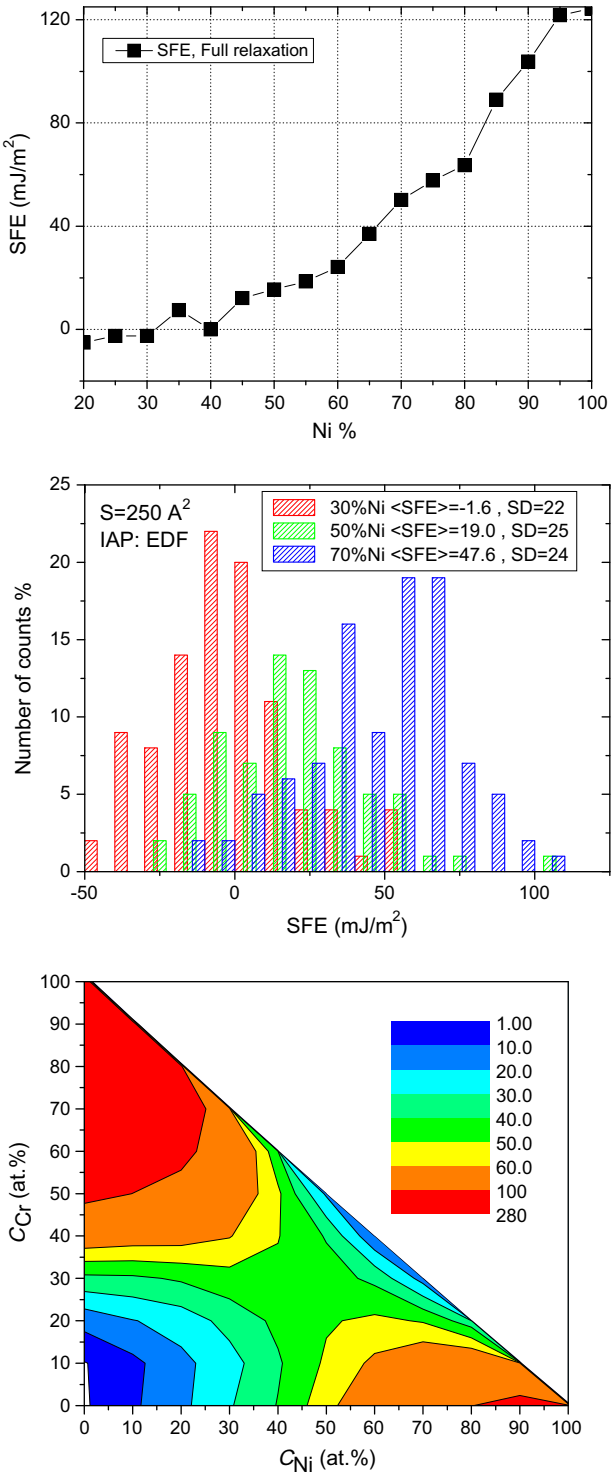

Fig. 1. (a) SFE in the position of stable stacking fault calculated using EDF potential (for the fault surface of ~20.000 Å^2) at 0 K. (b) The distribution of the SFE in Fe–*x*Ni alloys, calculated at 0 K using the EDF interatomic potential (IAP) for the surface (S) of fault of about 250 Å^2 (i.e. 16***b*** × 2***b***, this would correspond to the constriction of 2***b*** width made on a 4 nm loop). Each distribution is obtained for 500 runs varying initial distribution of Ni atoms. The abbreviation SD stands for standard deviation. (c) SFE (given in mJ/m^2) in the Fe–Ni–Cr as a function of composition [16]. In all the cases, SFE is calculated by generating a crystal containing a fault and using standard molecular static relaxation procedure, for details see [16].

2. Simulation techniques

The general computational methodology is exactly the same as applied in our previous work dealing with simulations in Fe–Ni alloys [13]. The interaction between a screw dislocation (SD) and interstitial FLs was studied using classical MD approach by applying shear deformation of $[-1-10](-111)$ type with a constant strain rate of 3×10^7 s^{-1} (resulting in the steady state velocity of

Table 1
Lattice parameters as a function of temperature.

T (K)	a_0 (Å)
303–306	3.52196
606–610	3.53254
902–908	3.54847

50 m/s). The crystallite, with axes oriented along [1 1 0], [1 −1 2] and [−1 1 1] directions, contained about 1.2M mobile atoms. Its dimensions along x, y and z were $40 \times 40 \times 10$ nm^3. An equilibrium lattice unit, a_0, was chosen appropriately to account for thermal expansion and its value is reported in Table 1. Periodic boundary conditions were applied along x and y directions, while atoms in a few outer $\pm z$ atomic layers were rigidly fixed in their positions. A screw dislocation with BV = 1/2[1 1 0] has been introduced according to the method applied by Rodney [10] and then relaxed using a combination of conjugate gradient and velocity quenching methods [17]. After the relaxation, the dislocation was dissociated in the (−1 1 1) plane into two Shockley partials located at a distance of about 10 nm from each other, which corresponds well to the value expected from the elasticity theory considerations.

An FL was introduced at a distance of ~10 nm away from the leading partial dislocation so that its geometrical center coincided with the dislocation glide plane. The three non-equivalent orientations of BV for each FL were inspected, and the case when BV = 1/3[−1 1 1] was excluded since the probability of the direct interaction with such loops is very low. We have considered circular Frank loops with a diameter of 2 and 5 nm. Due to the imposed periodic boundary conditions along the dislocation line, the center-to-center spacing between the loops was 40 nm, which corresponds to a volumetric density of 1.5×10^{22} m^{-3}. To explore both possibilities for the SD to approach the loop, we have performed simulations by applying positive and negative shear strain.

Integration of Newton's equations was performed using a constant time step equal to 5 fs. Calculations were done in the framework of a microcanonical *NVE* ensemble, where a number of atoms, N, system volume, V, and total energy, E, are conserved if the work of external forces is taken into account. The simulations were performed at 300, 600 and 900 K. The identification of the dislocation core and stacking fault atoms was realized by applying a combination of methods, namely: central symmetry analysis, common neighbor analysis, potential energy analysis and counting specific number of FCC neighbors.

Prior to study the interaction of the dislocation with FLs we have modeled its movement in the defect-free crystal to evaluate the friction stress, τ_f, which the dislocation experiences at the imposed strain rate. A smooth movement of the dislocation was seen at all studied temperatures, the width of the stacking fault ribbon was seen to vary (±25% from the average value) and no constrictions were seen to form on the dislocation line. Following the stress–strain curves, we could observe that increasing temperature reduces the instantaneous friction stress. The apparent friction stress τ_f was calculated by averaging the instantaneous resolved shear stress during the period within which the dislocation moves with the steady-state velocity for a distance of 40 nm (i.e. passes the whole crystal one time). The obtained τ_f are presented in Table 2. To validate the atom-core dislocation analysis we have measured the dislocation velocity in all simulation runs by tracking its position (as determined by the structural analysis) and compared it with the Orowan relationship linking strain rate with dislocation density, its Burgers vector and dislocation velocity i.e. $\dot{\gamma} = \rho b v$. A good agreement between the results is achieved (see Table 2) confirming consistency of geometrical parameters of the model, applied loading conditions and visualization techniques employed.

3. Results

MD simulations have been performed and the resulting stress–strain curves together with the atom-core visualization animations for every interaction mechanisms described below are attached to this paper as electronic supplementary material, which is the group of archived files. Root of each of the archived files contains a folder, whose name corresponds to the reaction type following the described below (see Section 3.1). Every folder contains subfolder, whose name refers to a specific reaction studied for a given BV orientation, loop size and simulation temperature. In this subfolder one finds the file named 'sscurve.gif', which is the stress–strain curve for a given reaction, and folder called 'vis_10video'. The latter contains three movies showing the interaction mechanism viewed along the three principal axes of the crystal i.e. [1 1 0], [1 −1 2] and [−1 1 1] vectors. By checking the evolution of dislocation-loop configurations from the three perspectives, it is easy to identify such important features as formation of constrictions, cross-slip movement and loop unfault, which is necessary in order to rationalize the interaction mechanism. We invite a reader to download the supplementary material offering an access to full details of the interaction mechanism for each simulated reaction, while in the next section several principal mechanisms observed will be described in detail and demonstrated by visualization snapshots.

3.1. Interaction mechanisms

All observed reactions have been subdivided into six groups depending on principal mechanisms involved and outcome products observed. A description of each type of the observed reaction mechanism is given below. Some of the interaction mechanisms have been observed in earlier studies in pure FCC metals [9,10] and in Fe–50Ni [13]. However, some new mechanisms have also been identified. In the following we illustrate a number of the interaction mechanisms as detected by atom-core visualization techniques. The evolution of the stress–strain relationships corresponding to the below described reactions is provided in Fig. 2.

(1) *Unfault with the formation of a 'full' helical turn*: The interaction process involving a 1/3[1 1 1] loop and a screw dislocation is illustrated in Fig. 3. In this configuration the loop is initially attracted to a leading partial (LP) dislocation, which bends towards the loop. Under the action of applied stress, the dislocation moves towards the loop and on the contact it forms the junction, see Fig. 3(a). While, the trailing partial (TP) dislocation reaches the junction, the LP unzips from the junction and cuts the loop, as shown in Fig. 3(b). The TP follows the LP so as the constriction is formed in the opposite side of the loop. At this step, the loop is splitted into upper and lower parts connected to the two dislocation arms, see Fig. 3(c). The lower part, attached to the 'right arm', is immediately reformed as a set of superjogs by the propagation of the D-Shockley dislocation [10] over the loop fault combined with the cross-slip of the constriction, see Fig. 3(d). The constriction on the 'left arm' is not yet formed. Its formation occurs with further increase of the applied stress up to 103 MPa (at

Table 2
Dislocation movement without defects.

T (K)	Yield stress (from MD) (MPa)	Steady-state velocity (from MD) (m/s)	Velocity from Orowan law (m/s)	Shear modulus (GPa)
300	96.8	47.0	43.7	70
600	56.4	49.9	43.8	69
900	37.2	48.9	45.2	61

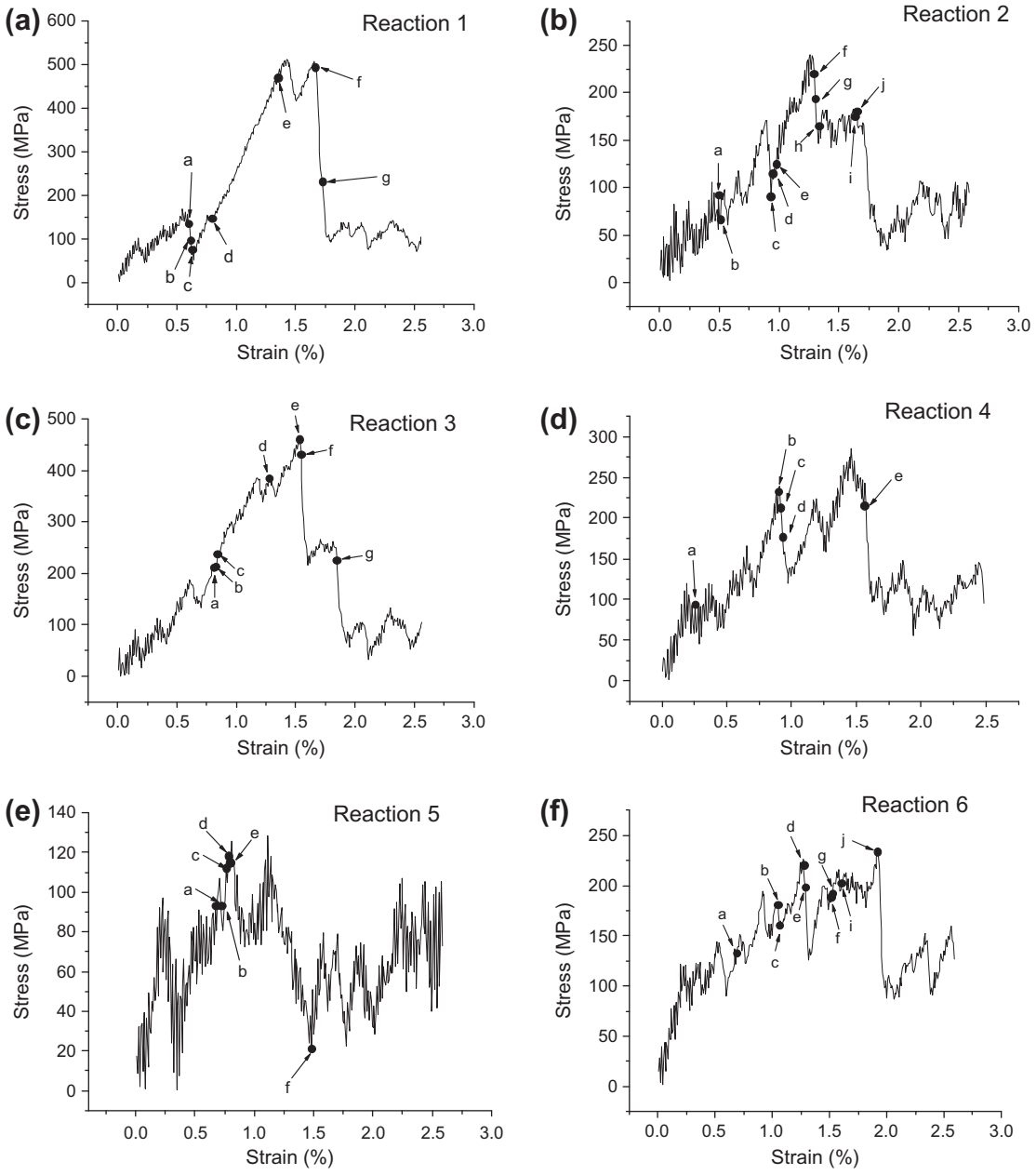

Fig. 2. Stress–strain curves obtained for the interaction according to mechanism (a)#1 (b)#2 (c)#3 (d)#4 (e)#5 (f)#6 (see Section 3.1). The letters refer to moments shown below in Fig. 3–8 for the reactions #1–#6, respectively.

T = 300 K), which triggers the removal of the extrinsic stacking fault in the same manner as for the lower part, see Fig. 3(e). Further increase of shear stress shrinks the set of segments dissociated in different {1 1 1} planes into a confined helical turn, see Fig. 3(e). The helical turn cannot move in the dislocation glide plane and the unpinning of the dislocation proceeds in two steps: (i) firstly, the LP arms form an edge dipole (see Fig. 3(f)) and close (see Fig. 3(g)), forming a straight 1/6<1 1 2> LP which propagates away from the loop increasing the area of the fault; (ii) then, the TP arms close in the same way, thus leaving behind a perfect ½<1 1 0> loop and closing the faulted area created by the LP.

(2) *Unfault with the formation of a 'bridge' segment*: This interaction mechanism was observed only for the small loops with BV = 1/3 [1 1 −1] at 600 K and 900 K. Initially, the LP is attracted to the loop and it moves towards the loop upon action of increasing shear stress. It forms the junction on the contact with the loop, see Fig. 4(a). The junction cross-slips downwards thus forming a 'bridge' connecting the LP with the top segment of the loop, see Fig. 4(b). The 'bridge' is made of several segments, being formed as a result of the dislocation cross-slip and re-dissociation in corresponding {1 1 1} planes. Then, the TP approaches and forms the constriction followed by the unfaulting of the bottom part of the loop, see Fig. 4(c). Eventually, the bridge is transformed into the helical turn, and correspondingly, the fault of the upper part of the loop is swept (thus, the superjog is formed), as shown in Fig. 4(d and e). With the applied stress the dislocation arms start to bow and conjunct via the closure of the dipole, see Fig. 4(f and g). Then two superjogs approach one another, see Fig. 4(h and i), and the TP unpins, see Fig. 4(j), leaving the perfect loop with BV = 1/2[1 1 0] behind the dislocation.

(3) *Shear with the formation of constriction*: The interaction of the screw dislocation with a 1/3[1 1 −1] loop can serve as an exam-

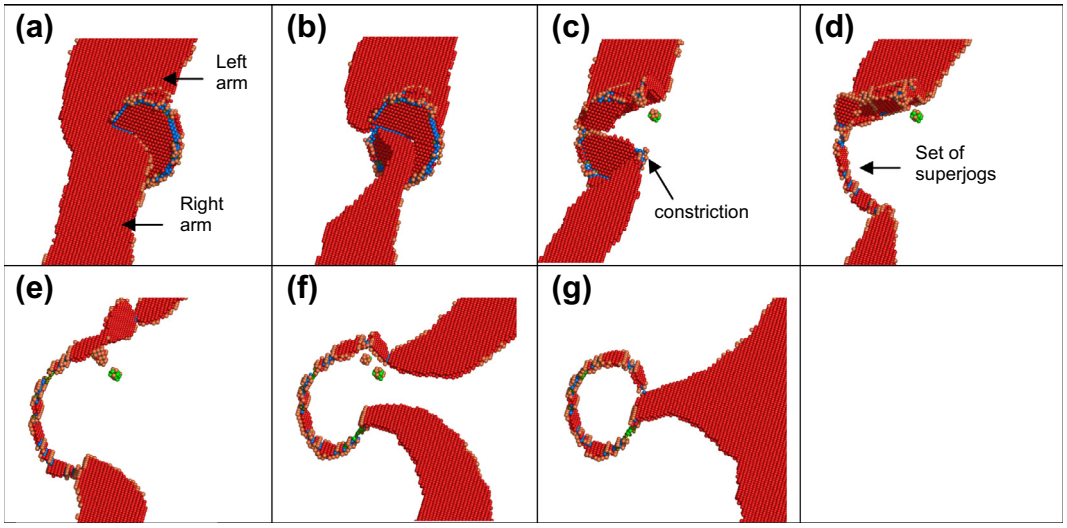

Fig. 3. Visualizations of the dislocation reaction #1 (D_L = 5 nm; BV = 1/3[1 1 1]; T = 300 K): snapshots taken at times: (a) 200 ps, (b) 205 ps, (c) 210 ps, (d) 265 ps, (e) 450 ps, (f) 555 ps and (g) 575 ps.

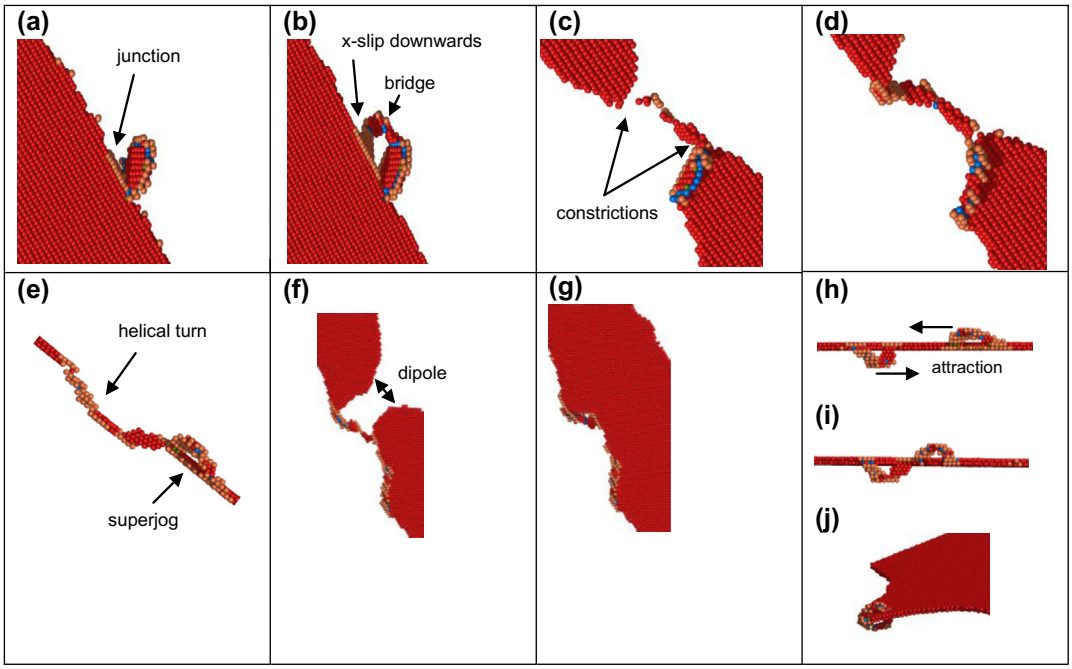

Fig. 4. Visualizations of the dislocation reaction #2 (D_L = 2 nm; BV = 1/3[11–1]; T = 600 K): snapshots taken at times: (a) 165 ps, (b) 170 ps, (c) 310 ps, (d) 315 ps, (e) 325 ps, (f) 430 ps, (g) 435 ps, (h) 445 ps, (i) 545 ps and (j) 550 ps.

ple of this type of interaction. The LP dislocation is attracted to the closest segment of the loop. Further increase of the stress pushes the TP to form a short constriction, see Fig. 5(a). The locally constricted node dissociates in (1 −1 1) plane and glides downwards along the loop side, again gets constricted at the bottom of the loop and re-dissociates in the original glide plane, see Fig. 5(b and c). It thus can be considered that the 'left arm' performed a double cross-slip movement and displaced underneath the loop being attached to the loop via two segments (dissociated in different {1 1 1} planes) connected by a constriction. The connecting configuration being sessile in the (−1 1 1) plane pins the left arm. Under increasing stress, both arms bow out and the 'left arm' eventually makes contact with the back side of the loop at 289 MPa, see Fig. 5(d). Further increase of shear stress results in the formation of an edge dipole (see Fig. 5(e)) and its closure reforming the straight LP, see Fig. 5(f). Finally, sufficiently high shear stress pushes back the double cross-slipped 'left arm' to join with the loop, as shown in Fig. 5(g) and the edge dipole closes leaving the faulted loop.

(3P) *Unfault after shear with formation of constriction*: The mechanism is similar to the one observed in the reaction #3. However, after the unpinning of the LP, the TP dipole is formed and its closure provokes loop unfaulting (see Fig. 5(g)). As a result, a perfect loop with BV = 1/2<1 1 0> is left behind the dislocation.

(3SJ) *Shear with formation of constriction and absorption of half loop*: The initial stage is the same as in reaction #3. Before the closure of the TP dipole the re-dissociated segment (shown in Fig. 5(c)) transforms into superjog on the left dislocation arm. This jog glides away from the preexisting loop as TP unpins leaving

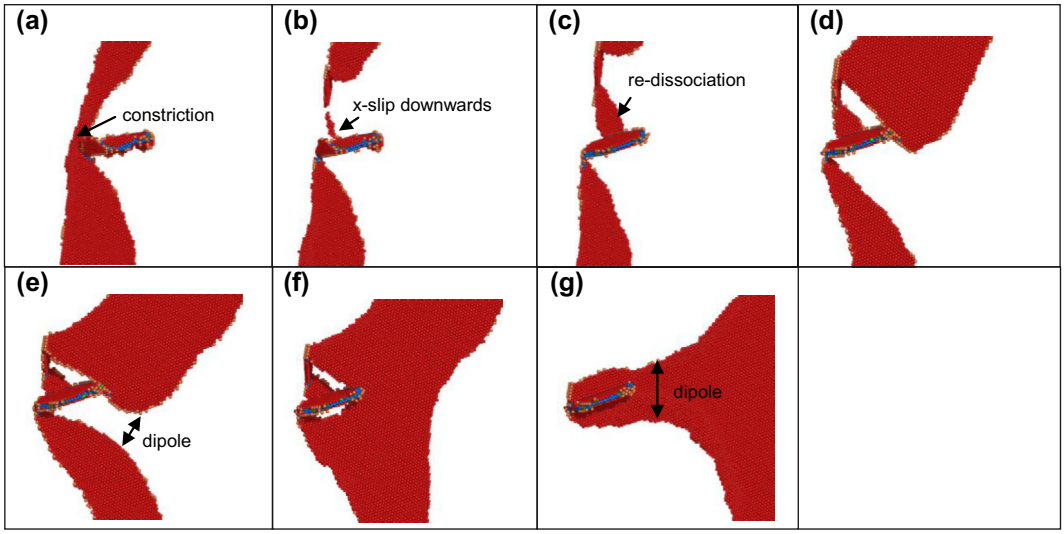

Fig. 5. Visualizations of the dislocation reaction #3 (D_L = 5 nm; BV = 1/3[1 1 −1]; T = 300 K): snapshots taken at times: (a) 270 ps, (b) 275 ps, (c) 280 ps, (d) 425 ps, (e) 510 ps, (f) 515 ps and (g) 615 ps.

half-absorbed faulted loop behind. The superjog has the same structure as the one observed in reaction #5 (see below).

(4) *Simple shear*: The interaction process involving a 1/3[1 −1 1] loop and a screw dislocation is illustrated in Fig. 6. The LP is attracted to the loop surface, see Fig. 6(a), at sufficiently high shear stress it approaches the loop, shears its fault and propagates further, see Fig. 6(b and c). The TP follows the same sequence of the basic steps, see Fig. 6(d). The unpinning of the TP from the loop occurs via the closure of the dipole, as is shown in Fig. 6(e). The sheared faulted loop with a step (a pair of stair-rod dislocations) on its surface is left behind. The step is however quickly removed recovering flat habit plane surface after the unpinning of the dislocation.

(4P) *Shear with unfaulting prior the unpinning of the TP*: The mechanism of the interaction is the same as in reaction #4. Prior to the unpinning of the TP (see Fig. 6(e)), the loop fault is removed by nucleation of the two partials on its surface, which sweep the fault The bottom and upper parts of the loop are disconnected from the left point (i.e. from junction with TP) and reorient in the other two {1 1 1} planes inclined in the (−1 1 1) glide plane. After that the TP unpins leaving a perfect loop with BV = 1/2<1 1 0> behind. Such reaction was observed only at high temperature.

(5) *Absorption into two glissile superjogs*: The interaction of the screw dislocation with a 1/3[1 −1 1] loop at T = 900 K can serve as the only example of this type of interaction. The LP is attracted to the loop and gets pinned on it, see Fig. 7(a). While the TP approaches the loop, the bottom part of the loop is already absorbed via the formation of D-Shockley partial, as is shown Fig. 7(b). At the moment the TP reaches the loop, the upper part of the loop also unfaults via the propagation of the D-Shockley dislocation, see Fig. 7(c–e). The two parts of the loop are now accommodated as glissile superjogs on the TP and LP dislocations. The whole configuration moves as the applied shear stress reaches 91 MPa, see Fig. 7(f). At this, the two superjogs are moving along dislocation line in opposite directions.

(6) *Absorption and reemission in the other {1 1 1} plane*: This reaction was observed only at 300 K for the interaction with a 1/3[1 −1 1] loop at T = 300 K. The LP is attracted by the loop and

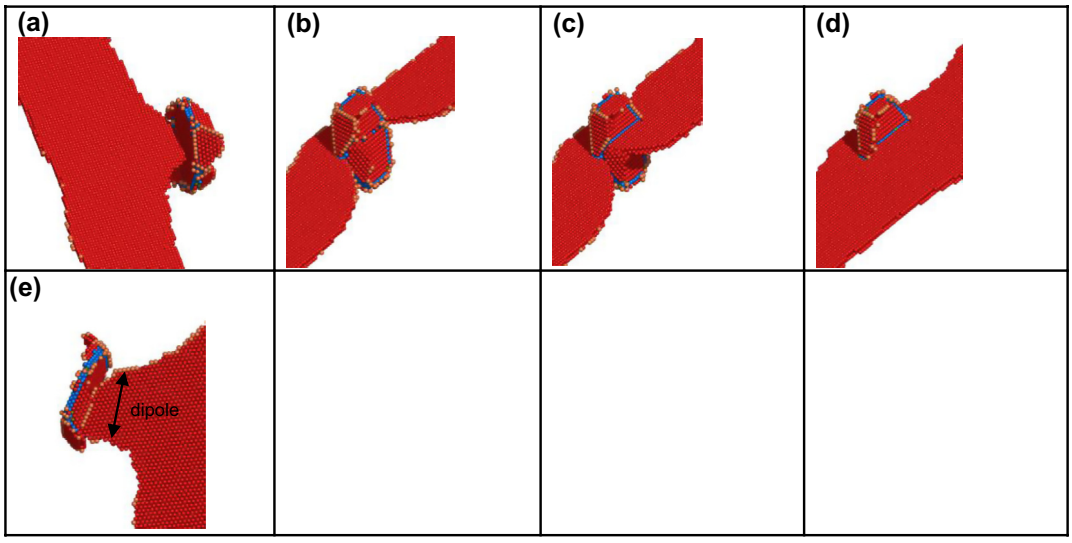

Fig. 6. Visualizations of the dislocation reaction #4 (D_L = 5 nm; BV = 1/3[1 −1 1]; T = 300 K): snapshots taken at times: (a) 85 ps, (b) 300 ps, (c) 305 ps, (d) 310 ps and (e) 520 ps.

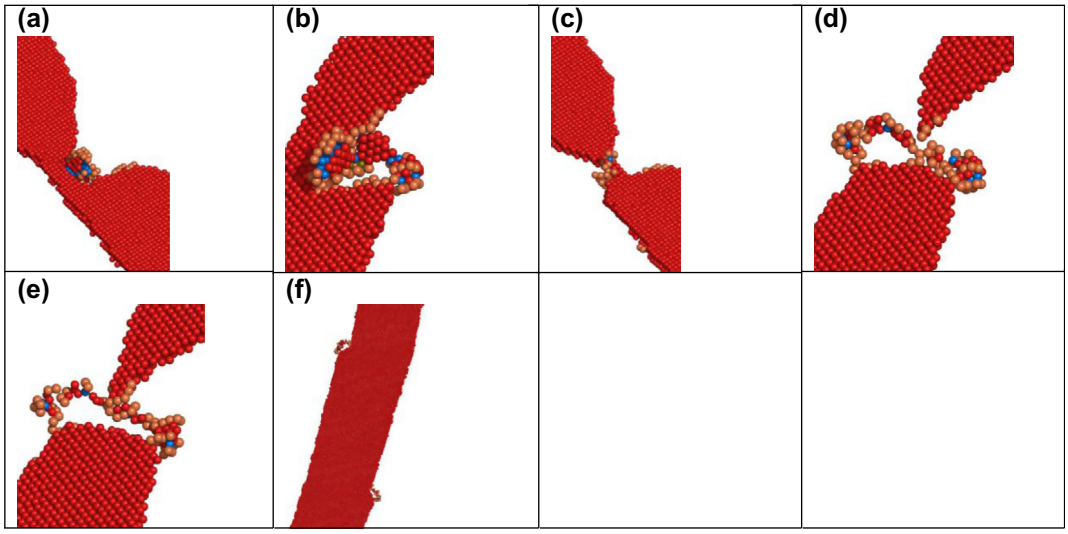

Fig. 7. Visualizations of the dislocation reaction #5 (D_L = 2 nm; BV = 1/3[1 −1 1]; T = 900 K): snapshots taken at times: (a) 225 ps, (b) 240 ps, (c) 255 ps, (d) 260 ps, (e) 265 ps and (f) 495 ps.

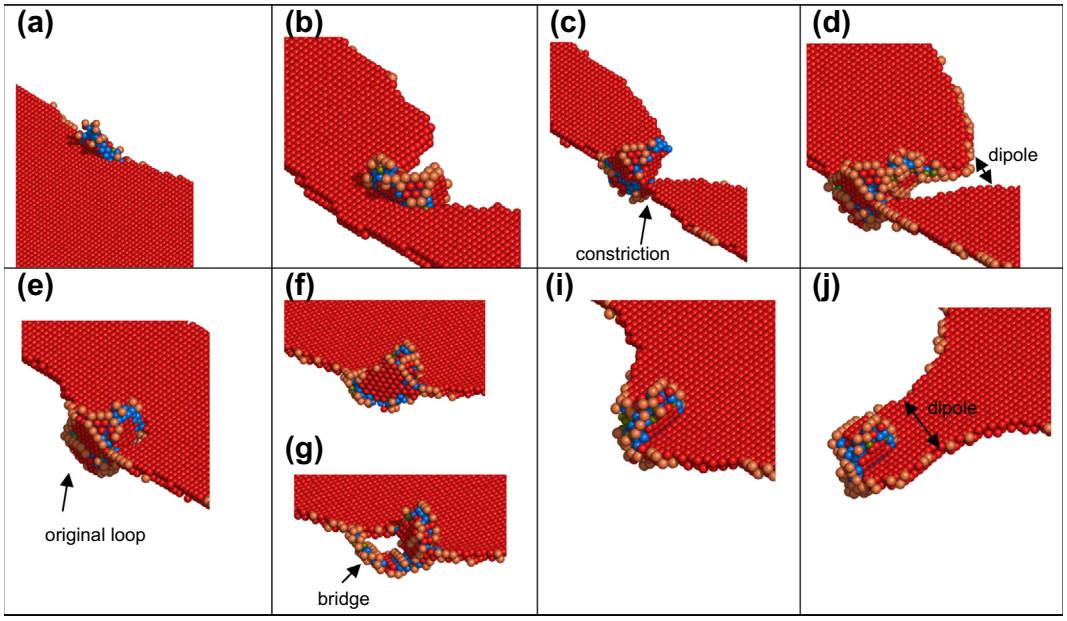

Fig. 8. Visualizations of the dislocation reaction #6 (D_L = 2 nm; BV = 1/3[1 −1 1]; T = 300 K): snapshots taken at times: (a) 230 ps, (b) 350 ps, (c) 355 ps, (d) 425 ps, (e) 430 ps, (f) 505 ps, (g) 510 ps, (h) 535 ps and (i) 640 ps.

moves towards it which results in its pinning, see Fig. 8(a). With increasing shear stress, the TP approaches the loop and forms a constriction across the loop surface, see Fig. 8(b and c). After that the constricted part of the dislocation re-dissociates in the loop habit plane, while the dislocation arms continue to bow, see Fig. R6(c). Then, the TP emerges a dipole which eventually closes, see Fig. 8(d and e). The pre-existing loop is now absorbed into the 'bridge' configuration on the TP, see Fig. 8(f and g). The bridge consists of multiple segments re-dissociated in different {1 1 1} planes, see Fig. 8(g). Then, the TP emerges a dipole, see Fig. 8(i and j), which closes leaving the faulted Frank loop in the (1 1 1) plane.

The type of the interaction mechanisms observed in the simulations referred to each the studied case is presented in Table 3 and the corresponding critical unpinning stress (τ_C) is given in Table 4. The same information is presented graphically in Fig. 9(a) and (b), for 2 and 5 nm FLs, respectively. The figure presents τ_C as a

Table 3
Classification of the interaction mechanisms observed for 2 and 5 nm FLs, referred to in the table as 'S' and 'L', respectively. In the reactions where negative shear strain was applied, a symbol '_m' is added in the coloumn 'FL size'.

Burgers vector of FLs	FL size	Temperature (K)		
		300	**600**	**900**
1/3[1 1 1]	**L**	1	1	1
	L_m	3P	3	3
	S	3	3	3
	S_m	3	3	3
1/3[1 1 −1]	**L**	3	3	3
	L_m	1	1	1
	S	3	3	3SJ
	S_m	1	2	2
1/3[1 −1 1]	**L**	4	4	4
	L_m	4	4	4
	S	4	4	5
	S_m	6	4	4P

Table 4
Critical unpinning stress (after subtraction of yield stress) measured in MPa for 2 and 5 nm FLs, referred to in the table as 'S' and 'L', respectively. In the reactions where negative shear strain was applied, a symbol '_m' is added in the coloumn 'FL size'.

Burgers vector of FLs	FL size	Temperature (K)		
		300	**600**	**900**
1/3[1 1 1]	**L**	415	368	365
	L_m	313	251	231
	S	163	126	104
	S_m	147	116	116
1/3[1 1 −1]	**L**	364	308	243
	L_m	398	354	290
	S	162	135	135
	S_m	207	183	134
1/3[1 −1 1]	**L**	189	169	142
	L_m	252	140	121
	S	112	98	91
	S_m	137	120	105

function of Burgers vector of FLs collected in three bars each corresponding to a certain simulation temperature.

First, we discuss the result obtained for the smaller loops. Among the well-established interaction mechanisms we list the following ones: absorption into a helical turn [10], simple shear [9] and absorption into two glissile superjogs [9]. We can see from Fig. 9(a) that in the case of 2 nm FL with BV = 1/3[1 1 1] temperature does not modify the interaction mechanism and the loop is sheared in all the cases (i.e. reaction #3 realizes). The similar interaction mechanism (and similar τ_C) is identified for half of the cases of FLs with BL = 1/3[1 1 −1] at 300 K. Loop unfaulting into a helical turn was observed for the other half of the cases at all the studied temperatures. Finally, FL with BV = 1/3[1 −1 1] interacts with the dislocation mainly via shear mechanism, whose details may vary depending on simulation temperature. This configuration offers the lowest resistance against the dislocation motion. The fact that the loop shear interaction requires rather low unpinning stress is also confirmed in our previous simulations in Fe–50Ni [13].

It is also worth noticing that for 5 nm loop, the unfault into a helical turn occurred in half of the studied cases for DLs with BV = 1/3[1 1 1] and 1/3[1 1 −1] (in the second half of cases reaction #3 (shear with the formation of constriction) – was identified). The simple shear was the only mechanism observed for FLs with BV = 1/3[1 −1 1]. In the case of large loops temperature did not have any essential influence on the interaction mechanism.

3.2. Loop strength

The unpinning stress, expressed in reduced units ($\mu b/L$, μ = 93 GPa, $b = 0.7a_0$, L = 40 nm-D_L, where D_L is the loop size), is shown in Table 5. Here, we used the isotropic shear modulus, while an anisotropic shear modulus for the <1 1 0>{1 1 1} type of load is ~60 GPa i.e. by a factor 1.5 lower. This means that for the data reported in Table 5, the maximum exerted stress (i.e. Orowan stress) should not exceed 0.65–0.75 μb/L, which is indeed the case. Moreover, we can clearly see that the Orowan stress realizes only in the case of unpinning from a helical turn, which implies loop absorption mechanism. This result is perfectly consistent with the early studies performed in pure Ni and Cu as well as in Fe–50Ni (see introduction for Refs.).

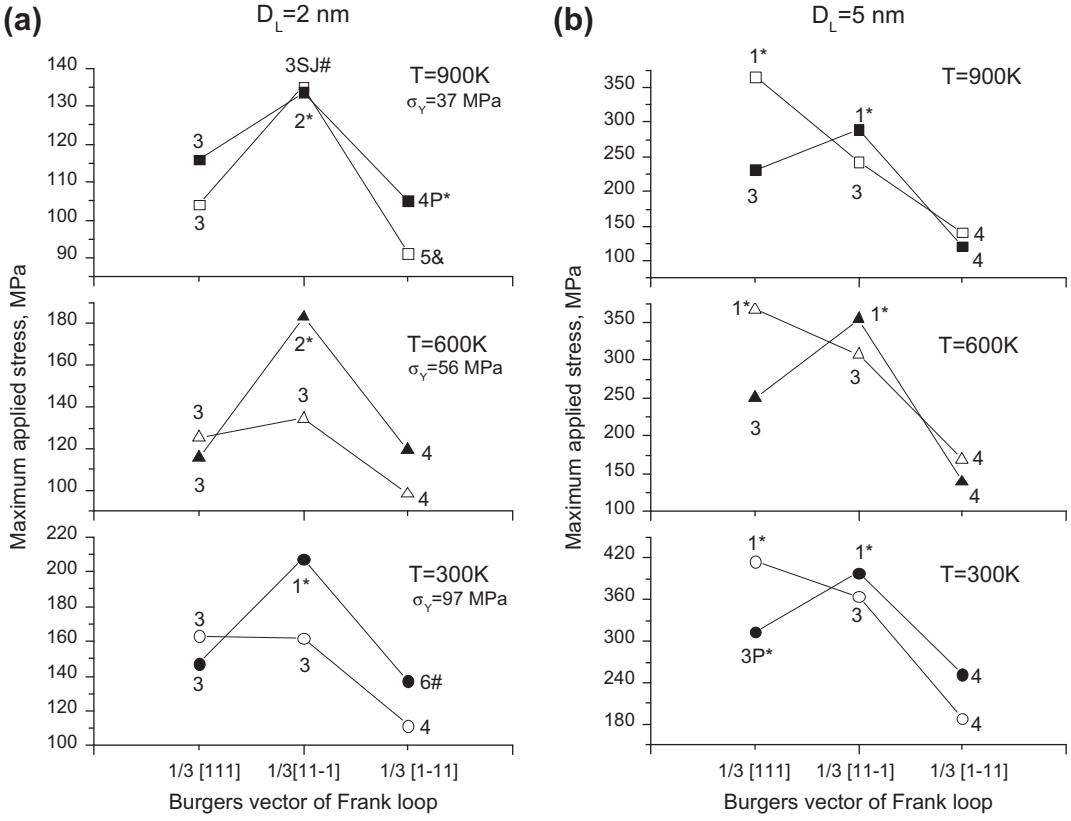

Fig. 9. τ_C as a function of Burgers vector of FL with size (a) 2 and (b) 5 nm. Three bars on each figure show the results obtained at 300, 600 and 900 K from down to top. The numbers next to the symbols on the figures refer to the type of the interaction mechanism (see Section 3.1). The latter one, which is marked with * and # symbols, implies, respectively, that the reaction led to the loop unfault or the loop structure was modified after the interaction but remained faulted. The reaction marked with & symbol led to the full absorption of the loop in the form of two superjogs. Open and filled symbols correspond to the direction of applied strain i.e. ½[1 1 0] and ½[−1 −1 0], respectively.

Table 5
Unpinning stress (subtracting yield stress) expressed in reduced units of $\mu b/L$ ($\mu b/L$, μ = 93 GPa, $b = 0.7a_0$, L = 40 nm-D_L, where D_L is the loop size).

Burgers vector of FLs	FL size	Unpinning stress (μb/L)		
		300	**600**	**900**
1/3[1 1 1]	**L**	0.65	0.58	0.58
	L_m	0.49	0.40	0.36
	S	0.27	0.21	0.17
	S_m	0.24	0.19	0.19
1/3[1 1 −1]	**L**	0.58	0.49	0.39
	L_m	0.64	0.57	0.46
	S	0.27	0.23	0.23
	S_m	0.35	0.31	0.22
1/3[1 −1 1]	**L**	0.28	0.25	0.21
	L_m	0.38	0.21	0.18
	S	0.18	0.16	0.15
	S_m	0.23	0.20	0.17

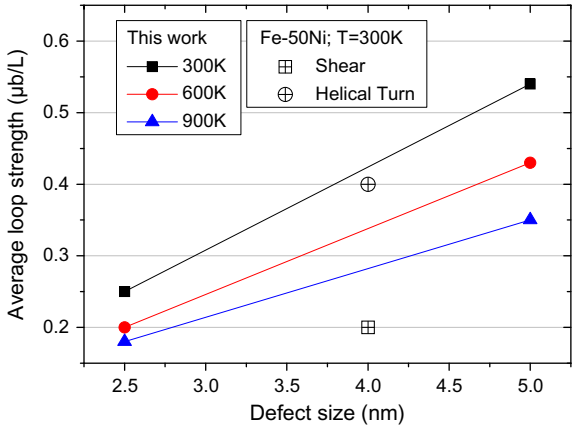

Fig. 10. Average τ_C measured for FLs in this work compared with average τ_C for loop shear and emission of a helical turn measured in Fe–50Ni at 300 K in [13]. The values for μ and L for the results from [13] are 80 GPa and 18 nm, respectively.

Finally, we compare the unpinning stresses measured in this work with the data obtained in Fe–50Ni for 4 nm Frank loops in [13]. Since the spacing of defects was different in the two simulations we compare τ_C using the reduced units. There are two interaction mechanisms which offer upper and lower bounds for the unpinning stress, namely: absorption into helical turn and loop shear. Therefore in Fig. 10, we plot τ_C corresponding to these two reactions in Fe–50Ni (obtained at 300 K) and compare them with the average τ_C measured at each studied temperature. The averaging is performed over τ_C values obtained for different interaction geometries. It clearly follows from Fig. 10 that τ_C for the emission of a helical turn in Fe–50Ni follows well the trend line based on the results obtained in Fe–10Ni–20Cr. While, the loop shear mechanism in Fe–50Ni offers much weaker resistance to dislocation glide. This comparison demonstrates the importance of the variation of the interaction mechanism on the hardening associated to the presence of Frank loops.

4. Summary and discussion

In this work we have studied the interaction of a screw dislocation with Franks loops of size 2 and 5 nm, in the temperature range 300–900 K in Fe–10Ni–20Cr FCC random alloy. The latter alloy is used as a model of 316-type austenitic steels, since the applied ternary interatomic potential has been especially developed to reproduce elastic constants and SFE of that steel. The interaction of a screw dislocation and Frank loops was characterized in terms of reaction mechanism and unpinning stress.

The results reveal six different interaction mechanisms about half of which lead to the unfaulting of a pre-existing loop. The unfaulting reactions are seen more often as temperature increases. This is consistent with temperature activated cross-slip mechanism [18] necessary to ensure the loop absorption. Thus with increasing test temperature the intensity of channel formation should raise. This also implies that the high SFE austenitic steels/alloys, where dislocations are easier to cross-slip, should have a lower resistance against channel formation. Since the unpinning stress in the case of the unfaulting reactions is regularly higher than for loop shear or reconstruction reactions (see the Section 3.1 for details), Frank loops will augment the flow stress more intensively (thus contributing to hardening) with increase of deformation temperature.

Previously, the interaction of dislocations with 4 nm Frank loops was studied in random Fe–50Ni and Fe–70Ni alloys with SFE ~20 and 50 mJ/m^2, respectively [13]. Only one possible interaction geometry leading to absorption into a helical turn was indentified and it was concluded that the absorption of loops is suppressed due to the high formation energy of a constriction. The latter is needed for the cross-slip movement of the dislocation line to promote loop unfaulting. The present calculations are also done in the low SFE alloy, however, much more frequent formation of constrictions and unfault events is observed. Correspondingly, the average strength of loops in Fe–10Ni–20Cr is also found to be higher in the present simulations.

We believe that the difference between the results obtained in Fe–50Ni and Fe–10Ni–20Cr comes from the amplitude of SFE variation as a function of local solute arrangement. As mentioned in introduction (see also Fig. 1), SFE variation is much stronger for the Fe–Ni potential developed in [19]. For such wide dispersion of SFE, the formation of somewhat extended constriction is extremely sensitive to the variation of local chemical arrangement and in practice hardly occurs for a sufficiently long dislocation segment to initiate loop unfaulting process.

5. Conclusions

Based on the above presented and discussed results we can draw the following conclusions:

1. Approximately half of the inspected configurations for dislocation-loop interaction lead to loop unfaulting, despite of rather low stacking fault energy of the alloy. The obstacle strength in reactions causing loop unfault is 0.5–0.65 μb/L, while it is ~0.2 μb/L in case of simple loop shear.
2. A new type of the interaction mechanism leading to the partial unfaulting and reconstruction of the Frank loops (but in a different {1 1 1} plane) was observed. Such reaction occurred only in the case of 2 nm loops. The strength of such interaction mechanism is of the order of 0.25 μb/L.
3. The primary feature controlling absorption in the alloy is the formation of short constrictions allowing for the local cross-slip dislocation movement. Strong local variation of SFE (such as in Fe–50Ni [13]) makes practically impossible the formation of constrictions on relatively large loops, preventing from loop unfault. Thus, magnitude of local variation of SFE is another factor to be accounted for in the consideration of dislocation-Frank loop interaction.

Acknowledgements

This work was performed in the framework of the EC-funded FP7/PERFORM60 project, under grant agreement 232612. Part of calculations has been performed at HPC Julich within the 'SORT' project. The research was partly supported by the FWO grant.

References

[1] G.S. Was, Fundamentals of Radiation Materials Science, Springer, New York, 2007.
[2] S.J. Zinkle, P.J. Maziasz, R.E. Stoller, J. Nucl. Mater. 206 (1993) 266.
[3] D.J. Bacon, Y.N. Osetsky, D. Rodney, Dislocation Obstacle Interactions at the Atomic Level, in: J.P. Hirth, L. Kubin (Eds.), Dislocation in Solids, 2010, p. 1 (Chapter 88).
[4] S.M. Bruemmer, E.P. Simonen, P.M. Scott, P.L. Andresen, G.S. Was, J.L. Nelson, J. Nucl. Mater. 274 (1999) 299.
[5] X.Q. Li, A. Almazouzi, J. Nucl. Mater. 385 (2009) 329.
[6] P.J. Maziasz, J. Nucl. Mater. 205 (1993) 118.
[7] I.M. Robertson, A. Beaudoin, K. Al-Fadhalah, L. Chun-Ming, J. Robach, B.D. Wirth, A. Arsenlis, D. Ahn, P. Sofronis, Mater. Sci. Eng., A 400–401 (2004) 245.
[8] J. Robach, I. Robertson, H. Lee, B. Wirth, Acta Mater. 54 (2006) 1679.
[9] T. Nogaret, C. Robertson, D. Rodney, Phil. Mag. 87 (2007) 945.
[10] D. Rodney, Acta Mater. 52 (2004) 607.
[11] C. Shin, H.H. Jin, J.H. Kwon, J.H. Shim, T.S. Byun, J. Korean Phys. Soc. 52 (2008) 1250.
[12] T. Nogaret, D. Rodney, M. Fivel, C. Robertson, J. Nucl. Mater. 380 (2008) 22.
[13] D. Terentyev, A. Bakaev, Y.N. Osetsky, Journal of Nuclear Materials, 2013, JNM_D_11_00728R3 (in press).
[14] G. Ackland, M. Mendelev, D. Srolovitz, S. Han, A. Barashev, J. Phys.: Condens. Matter. 16 (2004) 1.
[15] Y. Mishin, D. Farkas, M.J. Mehl, D.A. Papaconstantopoulos, Phys. Rev. B 59 (1999) 3393.
[16] G. Bonny, D. Terentyev, R.C. Pasianot, S. Ponce, A. Bakaev, Modell. Simul. Mater. Sci. Eng. 19 (2011).
[17] M. Allen, D. Tildesley, Computer Simulation of Liquids, Clarendon Press, Oxford, 1987.
[18] D. Hull, D.J. Bacon, Introduction to dislocations, Butterworth-Heinemann, Oxford, 2001.
[19] C. Becquart, Report F16O-CT-2003-508840, PERFECT IP Lille, 2005, pp. 22.